The Astrophysical Journal Letters, 963:L24 (13pp), 2024 March 1 https://doi.org/10.3847/2041-8213/ad2764

Roaring to Softly Whispering: X-Ray Emission after ∼3.7 yr at the Location of the Transient AT2018cow and Implications for Accretion-powered Scenarios*

Giulia Migliori[1], R. Margutti[2,3], B. D. Metzger[4,5], R. Chornock[2], C. Vignali[6], D. Brethauer[2], D. L. Coppejans[7], T. Maccarone[8], L. Rivera Sandoval[9], J. S. Bright[2,10], T. Laskar[11,12], D. Milisavljevic[13,14], E. Berger[15], and A. J. Nayana[2,16]

[1] INAF Istituto di Radioastronomia, via Gobetti 101, 40129 Bologna, Italy; giulia.migliori@inaf.it
[2] Department of Astronomy, University of California, Berkeley, Berkeley, CA 94720-3411, USA; rmargutti@berkeley.edu
[3] Department of Physics, University of California, Berkeley, 366 Physics North MC 7300, Berkeley, CA 94720, USA
[4] Department of Physics and Columbia Astrophysics Laboratory, Columbia University, New York, NY 10027, USA
[5] Center for Computational Astrophysics, Flatiron Institute, 162 5th Ave., New York, NY 10010, USA
[6] Dipartimento di Fisica e Astronomia "Augusto Righi", Università di Bologna, via P. Gobetti 93/2-40129 Bologna, Italy
[7] Department of Physics, University of Warwick, Coventry CV4 7AL, UK
[8] Department of Physics & Astronomy, Texas Tech University, Box 41051, Lubbock, TX 79409-1051, USA
[9] Department of Physics and Astronomy, University of Texas Rio Grande Valley, Brownsville, TX 78520, USA
[10] Astrophysics, Department of Physics, University of Oxford, Keble Road, Oxford OX1 3RH, UK
[11] Department of Physics & Astronomy, University of Utah, Salt Lake City, UT 84112, USA
[12] Department of Astrophysics/IMAPP, Radboud University, P.O. Box 9010, 6500 GL, Nijmegen, The Netherlands
[13] Purdue University, Department of Physics and Astronomy, 525 Northwestern Ave, West Lafayette, IN 47907, USA
[14] Integrative Data Science Initiative, Purdue University, West Lafayette, IN 47907, USA
[15] Center for Astrophysics, Harvard & Smithsonian, 60 Garden Street, Cambridge, MA 02138-1516, USA
[16] Indian Institute of Astrophysics, II Block, Koramangala, Bangalore 560034, India
Received 2023 October 2; revised 2024 January 31; accepted 2024 February 6; published 2024 February 26

Abstract

We present the first deep X-ray observations of luminous fast blue optical transient (LFBOT) AT 2018cow at ∼3.7 yr since discovery, together with the reanalysis of the observation at $\delta t \sim 220$ days. X-ray emission is significantly detected at a location consistent with AT 2018cow. The very soft X-ray spectrum and sustained luminosity are distinct from the spectral and temporal behavior of the LFBOT in the first ∼100 days and would possibly signal the emergence of a new emission component, although a robust association with AT 2018cow can only be claimed at $\delta t \sim 220$ days, while at $\delta t \sim 1350$ days contamination of the host galaxy cannot be excluded. We interpret these findings in the context of the late-time panchromatic emission from AT 2018cow, which includes the detection of persistent, slowly fading UV emission with $\nu L_\nu \approx 10^{39}$ erg s^{-1}. Similar to previous works (and in analogy with arguments for ultraluminous X-ray sources), these late-time observations are consistent with thin disks around intermediate-mass black holes (with $M_\bullet \approx 10^3$–$10^4\,M_\odot$) accreting at sub-Eddington rates. However, differently from previous studies, we find that smaller-mass black holes with $M_\bullet \approx 10$–$100\,M_\odot$ accreting at $\gtrsim$the Eddington rate cannot be ruled out and provide a natural explanation for the inferred compact size ($R_{\rm out} \approx 40\,R_\odot$) of the accretion disk years after the optical flare. Most importantly, irrespective of the accretor mass, our study lends support to the hypothesis that LFBOTs are accretion-powered phenomena and that, specifically, LFBOTs constitute electromagnetic manifestations of super-Eddington accreting systems that evolve to $\lesssim$Eddington over a ≈100-day timescale.

Unified Astronomy Thesaurus concepts: Accretion (14); Stellar accretion disks (1579); Supernovae (1668); Black holes (162); High energy astrophysics (739); X-ray astronomy (1810); Transient sources (1851); X-ray transient sources (1852)

1. Introduction

High-cadence, wide-area optical surveys have recently led to the discovery of a new class of luminous transients (peak bolometric luminosity $L_{\rm pk} \approx 10^{41}$–$10^{44}$ erg s^{-1}), characterized by rapid rising times ($t_{\rm rise} < 10$ days) and blue colors that are signatures of high effective temperatures $>10^4$ K. The class of fast blue optical transients (FBOTs; Drout et al. 2014)[17] collects a few tens of systems (e.g., Poznanski et al. 2010; Drout et al. 2014; Arcavi et al. 2016; Pursiainen et al. 2018; Tampo et al. 2020; Ho et al. 2022c). While the observational properties of FBOTs are heterogeneous and most likely reflect some intrinsic diversity among the transients, their fast rise times, high luminosities, and lack of ultraviolet (UV) line blanketing cannot be easily explained with the radioactive decay of newly synthesized ^{56}Ni as for ordinary supernova (SN) explosions. This argument especially applies to the most optically luminous end of the FBOT population (luminous FBOTs (LFBOTs)), which shows extreme peak luminosities

* Based on observations obtained with XMM-Newton, an ESA science mission with instruments and contributions directly funded by ESA Member States and NASA.

[17] Also referred to in the literature as fast evolving luminous transients (Rest et al. 2018).

reaching $L_{\rm pk} \approx 10^{44}$ erg s^{-1} combined with the shortest rise times of just a few days.

The key observational properties and inferences on the subclass of LFBOTs are summarized as follows: (i) Differently from FBOTs, LFBOTs are intrinsically rare events (local volumetric rate $\lesssim$1% of the core-collapse SN rate; Ho et al. 2020; Coppejans et al. 2022). (ii) These studies also revealed that LFBOTs have luminous X-ray and radio counterparts, sometimes as luminous as long gamma-ray bursts (LGRBs), and that, similar to GRBs, (iii) LFBOTs are capable of launching relativistic outflows, which implies the presence of a compact object (black hole (BH) or neutron star (NS), preexisting or newly formed). (iv) LFBOTs show highly time-variable nonthermal X-ray (and optical) emission (Rivera Sandoval et al. 2018; Margutti et al. 2019; Ho et al. 2022b), similar to GRB afterglows and tidal disruption events (TDEs), and clearly distinct from X-ray SNe that are powered by the shock interaction with the circumstellar medium (CSM). (v) LFBOTs are surrounded by dense but radially confined CSM, as revealed by their rapidly declining radio light curves (Ho et al. 2020, 2020; Nayana & Chandra 2021; Bright et al. 2022) and potential infrared "dust echo" signatures (Metzger & Perley 2023). (vi) In stark contrast with GRBs, the optical spectra of LFBOTs show the presence of H, demonstrating that LFBOTs are H-depleted but not H-free (e.g., Margutti et al. 2019; Perley et al. 2019). (vii) Finally, LFBOTs preferentially occur in low-mass star-forming galaxies, thus showing a preference for low-metallicity environments, and hence suggesting a connection with massive stars (Lyman et al. 2020; Coppejans et al. 2022; Yao et al. 2022).[18]

Physical scenarios to explain the LFBOT population fall under two broad categories: those invoking the interaction of a shock with a dense CSM as a way to efficiently convert the outflow's kinetic energy into radiation, and those involving the presence of energy injection by a "central engine" (e.g., Prentice et al. 2018; Margutti et al. 2019; Perley et al. 2019). In this second class of models, LFBOTs could be powered by a newly formed, rapidly rotating magnetar (e.g., Vurm & Metzger 2021); an accreting BH (e.g., Akashi & Soker 2021; Gottlieb et al. 2022) born in a failed blue supergiant star explosion (Quataert et al. 2019; Antoni & Quataert 2022); and TDEs by intermediate-mass BHs (IMBHs; e.g., Kuin et al. 2019; Perley et al. 2019). Recently, Metzger (2022) showed that LFBOTs could also result from the binary merger of a Wolf–Rayet star with its BH or NS companion. While pure CSM interaction models (e.g., Fox & Smith 2019; Schrøder et al. 2020; Leung et al. 2021; Dessart et al. 2022; Margalit 2022; Pellegrino et al. 2022) struggle to explain the mildly relativistic ejecta, rapid variability timescales, and nonthermal X-ray spectra of LFBOTs, it is important to note that the two sets of models (i.e., "interaction" vs. "central engine") are not mutually exclusive, and different parts of the spectrum can be dominated by different physical mechanisms (e.g., the radio emission could be shock–CSM interaction powered, while the rest of the spectrum is not).

Located in the spiral arm of the dwarf star-forming galaxy CGCG 137−068 at a distance $d \sim 60$ Mpc, AT 2018cow is the nearest LFBOT discovered so far (Prentice et al. 2018; Smartt et al. 2018; Perley et al. 2019) and offers an unparalleled opportunity to test and constrain the scenarios above. AT 2018cow has been extensively observed across the entire electromagnetic spectrum (Kuin et al. 2019; Rivera Sandoval et al. 2018; Ho et al. 2019; Margutti et al. 2019; Perley et al. 2019; Nayana & Chandra 2021). The observational findings from these campaigns that are most relevant to our study are summarized below.

AT 2018cow displayed luminous, highly variable X-ray emission (peak $L_{\rm X} > 10^{43}$ erg s^{-1}) of *nonthermal* origin with two spectral components: a persistent, relatively hard power law ($F_\nu \propto \nu^{-0.6}$) at $h\nu > 0.1$ keV, and a transient Compton hump feature dominating at $h\nu > 10$ keV at $\delta t < 10$ days (Rivera Sandoval et al. 2018; Margutti et al. 2019). While the bright radio to millimeter emission of AT 2018cow stems from a nonrelativistic shock interaction with a dense medium (Ho et al. 2019; Margutti et al. 2019; Nayana & Chandra 2021), the persistent optical/UV blue colors requiring $T_{\rm eff} \approx 15{,}000$ K weeks after discovery (e.g., Margutti et al. 2019; Perley et al. 2019; Xiang et al. 2021), and the broadband X-ray properties above demand a different powering source, which can be in the form of a long-lived central engine. Slowly decaying, luminous ($L > 10^7\,L_\odot$) UV emission years after discovery has been recently reported by Sun et al. (2022, 2023), Chen et al. (2023a, 2023b), Inkenhaag et al. (2023), and Mummery et al. (2024), and similarities have been noted with radiation powered by accretion processes on compact objects. Along the same lines, a high-frequency (224 Hz) quasi-periodic oscillation (QPO) feature in the X-ray timing properties of AT 2018cow supports the presence of a compact object, either an NS or a BH with mass $M < 850\,M_\odot$ (Pasham et al. 2021; but see also Zhang et al. 2022). While no evidence was found for a long-lived relativistic jet such as those of GRBs (Bietenholz et al. 2020; Mohan et al. 2020), panchromatic observations of AT 2018cow further indicated a complex geometry that strongly departs from spherical symmetry, as was directly confirmed by the very large optical polarization (∼7%) at early times (Maund et al. 2023).

Here we present deep X-ray observations of AT 2018cow performed up to ≈3.7 yr after the optical discovery, and we discuss the implications of a late-time X-ray detection on the intrinsic nature of this new class of transients. The paper is organized as follows: In Sections 2 and 3 we present the analysis of the XMM-Newton and NuSTAR observations at $\delta t \geqslant 218$ days. We put the X-ray data into the broader context of the late-time emission from AT 2018cow in Sections 4 and 5, and we discuss our findings in Section 6. We conclude in Section 7. In the Appendix we provide an analysis of Chandra HETG observations at $\delta t = 8.2$ days that has not been published elsewhere. Times are referred to the epoch of the optical discovery, which is MJD 58285.44, and we adopt a luminosity distance of 60 Mpc (Prentice et al. 2018; Smartt et al. 2018; Perley et al. 2019).

2. Late-time XMM-Newton Follow-up

Since its discovery, AT 2018cow has been targeted four times by XMM-Newton (PI Margutti). The first two epochs (Obs1 and Obs2) were presented in Margutti et al. (2019). Here we report the analysis of the 2019 observation (Obs3, $\delta t \sim 218$ days, Obs ID 0822580601) and the 2022 one (split in three, $\delta t \sim 1349$–1358 days; Obs4a, Obs4b, Obs4c, collectively Obs4; Obs IDs: 0843550401, 0843550501, 0843550601),

[18] The lack of evidence of cooling of LFBOTs like AT2018cow makes them phenomenologically distinct from the new class of luminous, fast-cooling transients, which occur in early-type galaxies and have no detected X-ray or radio emission (Nicholl et al. 2023).

Table 1
XMM-Newton Observations

Observation Log				
	Obs3	Obs4		
	0822580601	0843550401 (Obs4a)	0843550501 (Obs4b)	0843550601 (Obs4c)
Date (YYYY-mm-dd)	2019-01-20	2022-02-24	2022-03-01	2022-03-05
MJD	58503.2	59634.4	59639.1	59643.6
Time since discovery (d)	218	1349	1354	1358
Duration (ks)	56.4	39.3	44.6	44.6
Exposure (ks)	42.5(pn)	31.2(pn)	7.6(pn)	2.2(pn)
	54.2(MOS1)	37.4(MOS1)	14.0(MOS1)	15.3(MOS1)
	54.4(MOS2)	37.4(MOS2)	17.0(MOS2)	23.4(MOS2)
AT 2018cow Detection				
	Obs3		Obs4	
0.2–4.5 keV net count rate (counts s^{-1})	$(9.4 \pm 3.2)\times10^{-4}$ (pn)		$(5.7 \pm 2.4)\times10^{-4}$ (pn)	
	$(2.5 \pm 1.4)\times10^{-4}$ (MOS1)		$(7.1 \pm 1.9)\times10^{-4}$ (MOS1)	
	$(4.5 \pm 1.5)\times10^{-4}$ (MOS2)		$(2.7 \pm 1.3)\times10^{-4}$ (MOS2)	
	$(11.3 \pm 3.0)\times10^{-4}$ (tot.)		$(6.3 \pm 2.0)\times10^{-4}$ (tot.)	
Detection likelihood	10.8		9.1	
0.3–10 keV unabs. flux (erg cm^{-2} s^{-1})	$(4.5^{+1.5}_{-1.4})\times10^{-15}$		$(1.0 \pm 0.4)\times10^{-15}$	
0.3–10 keV luminosity (erg s^{-1})	$(1.9 \pm 0.6)\times10^{39}$		$(4.3 \pm 1.7)\times10^{38}$	

Note. Detection count rates and likelihood have been obtained with `edetect_chain` (Obs3) and `edetect_stack` (Obs4); see Section 2. The count rates are calculated under the entire PSF of the detection, corrected for background, vignetting, detector efficiency, and gaps. Unabsorbed fluxes have been derived from the spectral analysis for Obs3 and from the pn count rate using WebPIMMS for Obs4. In both cases, we used the spectral parameters from the best-fitting power-law model of Obs3 ($\Gamma = 2.9$ and $N_{\rm H,MW} = 5 \times 10^{20}$ cm^{-2}).

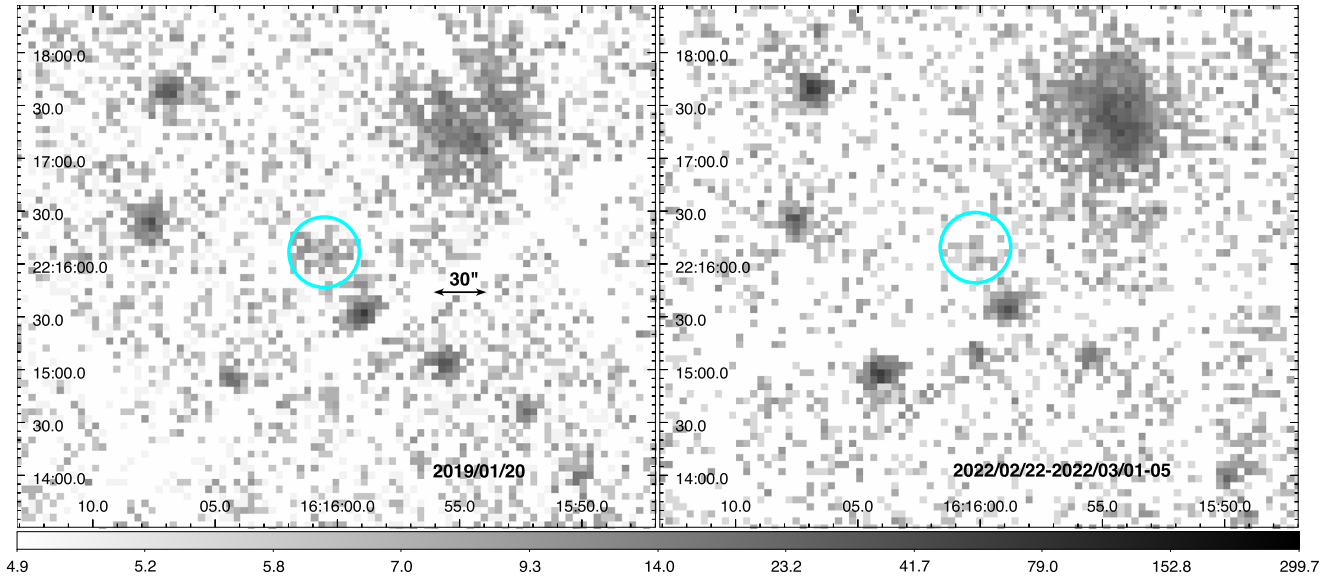

Figure 1. Mosaic of the 0.2–4.5 keV images of AT 2018cow in the three EPIC cameras for Obs3 (left panel) and Obs4 (right panel). Color intensity scales logarithmically with the number of counts. The cyan circle ($r = 20''$) marks the XMM-Newton detection.

which sample the very late time X-ray evolution of an FBOT (Table 1).

We reduced and analyzed the data of the three EPIC cameras, pn, MOS1, and MOS2, using the Scientific Analysis System (SAS) v. 20.0.0 and calibration files CALDB 3.13. Obs4b and Obs4c were significantly impacted by high-background flares, while Obs3 and Obs4a were not. For the former, optimized flare filtering was achieved with `espfilt`,[19] which led to a severe reduction in the effective exposure time, especially for the pn camera (Table 1).

2.1. Source Detection

An X-ray source is clearly visible at the location of AT 2018cow in the 0.2–10 keV image of Obs3 (see

[19] https://xmm-tools.cosmos.esa.int/external/sas/current/doc/espfilt/espfilt.html

Figure 1). We restricted our analysis to the 0.2–4.5 keV energy range (i.e., bands 1–4 of the XMM catalogs) since above ≈5 keV the background dominates. We estimated the background contribution from several source-free circular regions around AT 2018cow and in the same chip. In the 0.2–4.5 keV pn image, which has the best statistics, we measured 41 ± 14 net counts in a 20″ circular region centered at the optical coordinates of AT 2018cow. To assess the significance of the detection, we ran the task `edetect_chain` for all three cameras simultaneously over the full 0.2–4.5 keV energy band and in four sub–energy bands (i.e., 0.2–0.5 keV, 0.5–1.0 keV, 1.0–2.0 keV, and 2.0–4.5 keV). The source is significantly detected in the full 0.2–4.5 keV with a resulting detection maximum likelihood `DET_ML`=10.8 ($\gtrsim 3\sigma$, Gaussian equivalent). The 0.2–4.5 keV net count rates for each instrument are reported in Table 1. The analysis of the distribution of the counts in the energy sub-bands shows that most counts are clustered below 2 keV.

The centroid coordinates of the X-ray source in Obs3 are R.A. = 244.00104 deg, decl. = 22.26758 deg with a positional uncertainty of 1.″5, fully consistent with the coordinates of the optical counterpart. Note that the X-ray source closest to AT 2018cow is at 38″ and its flux did not vary through the XMM-Newton observations, suggesting a negligible level of contamination. The detection of AT 2018cow in XMM Obs3 has been previously reported by Yao et al. (2022).[20] A source is present also in the fourth XMM-Newton serendipitous source catalog (4XMM, data release 11 (DR11); Webb et al. 2020); instead, the nondetection claimed in Pasham et al. (2021) is likely due to the use of the MOS1 image alone.

From visual inspection, no source is apparent in the individual images of the three exposures of Obs4. To maximize our sensitivity to faint sources, we ran the SAS task `edetect_stack`, which performs source detection on stacked images from different exposures (Traulsen et al. 2019, 2020). Following a similar argument to that for Obs3, we restricted our analysis to ⩽5 keV. We find evidence for a point-like[21] X-ray source with a combined EPIC detection likelihood[22] `DET_ML` = 9.1 (3.8σ Gaussian equivalent) in the 0.2–4.5 keV energy band. However, the source position is displaced 4.″4 north (R.A.:244.00079 deg, decl.: 22.26925 deg) with respect to the optical position of AT 2018cow. The 1σ positional error is 1.″9, and Traulsen et al. (2019) quote a mean systematic error in the range 0.″43–0.″73, hence an offset of ∼2σ from the optical position. We note that the X-ray position is also 5.″5 offset from the host galaxy centroid. Inspection of the `edetect_stack` intermediate steps shows that this offset is the result of the final maximum likelihood fitting performed by the `eml_detect` task, while the input position provided in the previous step by the `ebox_detect` task is within 2″ from the AT 2018cow position, suggesting that uncertainties in merging the images or performing the point-spread function (PSF) fitting may affect the final position (see, e.g., Rosen et al. 2016; Webb et al. 2020). The 0.2–4.5 keV net count rates are reported in Table 1.

[20] This work focuses on the FBOT AT2020mrf; the detection of AT 2018cow is reported in the Appendix.

[21] The task assigns a zero source extent if the likelihood of the source being extended falls below a threshold of 4 or its extent radius falls below 6″ (Traulsen et al. 2019).

[22] This is defined as equivalent likelihood, i.e., the detection likelihood of the source in n individual images; see Equation (3) in Traulsen et al. (2019).

2.2. X-Ray Spectral Analysis

For Obs3, we extracted source spectra using data acquired by the three cameras. We used a source region with radius defined as the best-fitting radius for each camera determined by the detection tool and selected multiple, contiguous and source-free regions for the background. We employed the W-stat statistic and simultaneously fit the source and background spectra. We tested two spectral models, a power-law model and a blackbody model, both combined with an absorption component (i.e., `tbabs*pow` and `tbabs*bbody`). Unsurprisingly, given the low-number counts, the two models are statistically indistinguishable. We derived a very soft best-fitting power-law photon index of $\Gamma = 2.9^{+0.6}_{-0.4}$, whereas we obtained a best-fitting blackbody temperature of $kT = 0.16^{+0.04}_{-0.03}$ keV. In both cases, no evidence for intrinsic absorption is found, and we thus froze the $N_{\rm H}$ to the Galactic value $N_{\rm H,MW} = 0.05 \times 10^{22}\,{\rm cm}^{-2}$ (Kalberla et al. 2005). This is in line with upper limits derived from high-count spectra at early times ($N_{\rm H,int} < 0.02 \times 10^{22}\,{\rm cm}^{-2}$; Margutti et al. 2019). We further explored a multicolor blackbody disk model (`diskbb`), which is the implementation of the standard Shakura & Sunyaev (1973) thin-disk model. The inner disk temperature is constrained to $T_{\rm in} = 0.23^{+0.06}_{-0.04}$ keV, while for the inner disk radius we infer a maximum value, $R_{\rm in} \lesssim 1340$ km for a face-on disk. The UV flux predicted by this model fails to explain the observed emission from AT 2018cow, and we refer the reader to Section 5 for a self-consistent UV to X-ray multicolor blackbody disk modeling. Fitting with a thermal plasma model (`apec`) leads to an extremely low temperature ($kT \sim 0.009$ keV) and to a worse fit.

To conclude, while the Obs3 data cannot constrain the spectral shape in detail, there is a clear indication of a spectral softening of the X-ray emission at $\delta t \geqslant 210$ days, which signals a change with respect to the persistently hard X-ray emission with $\Gamma \sim 1.5$ observed at $\delta t \leqslant 82$ days (Rivera Sandoval et al. 2018; Margutti et al. 2019, Figure 2). The 0.3–10 keV unabsorbed flux inferred from the spectral analysis ranges from $(3.1\ ^{+3.5}_{-1.6}) \times 10^{-15}$ erg cm^{-2} s^{-1} (blackbody model) to $(4.5 \pm 1) \times 10^{-15}$ erg cm^{-2} s^{-1} (power-law model). Note that the higher flux of $F_{\rm X} \sim 1.6 \times 10^{-14}$ erg cm^{-2} s^{-1} reported in Yao et al. (2022) for this observation is the result of the harder $\Gamma \approx 2.0$ that was *assumed* by the authors.

While the limited statistics of Obs4 also leave the spectral models unconstrained, we note that most of the counts in the source region are at energies ⩽2 keV, which supports the conclusion of spectral softening of the source. Using the output of the detection algorithm, we estimated the hardness ratios (HR) in the 0.2–1 keV (b1), 1–2 keV (b2), and 2–4.5 keV (b3) energy bands for the pn data. For $\mathrm{HR1} = (\mathrm{b2} - \mathrm{b1})/(\mathrm{b2} + \mathrm{b1})$ and $\mathrm{HR2} = (\mathrm{b3} - \mathrm{b2})/(\mathrm{b2} + \mathrm{b3})$, we obtained $\mathrm{HR1} = -0.4 \pm 0.5$ and $\mathrm{HR2} = -0.1 \pm 0.5$, respectively, which are in rough agreement with the values in Obs3 ($\mathrm{HR1} = -0.9 \pm 0.4$ and $\mathrm{HR2} = -1.0 \pm 0.6$), although, given the large uncertainties, the HR measurements should be considered as purely indicative. Assuming $\Gamma = 2.9$ as derived from Obs3, the pn count rate of Obs4 converts into an unabsorbed 0.3–10 keV flux of $F_{\rm X} \approx (1.0 \pm 0.4) \times 10^{-15}$ erg cm^{-2} s^{-1} (Table 1).

3. Late-time NuSTAR Follow-up

We obtained deep observations of AT 2018cow with the Nuclear Spectroscopic Telescope Array (Harrison et al. 2013) on 2022 March 2 (Program #084355; PI Margutti; $\delta t = 1354.6$ days). NuSTAR observations were processed using `NuSTARDAS` v1.9.7 and the NuSTAR `CALDB` released on 2022 May 10. Part of our observations were severely affected by solar activity. Filtering out periods of increased detector background with `saacalc = 3`, `saamode = strict`, `tentacle = yes` leads to effective exposures of ≈113 and ≈111 ks on modules A and B, respectively. No source of significant hard X-ray emission is detected at the location of AT 2018cow. Using extraction regions that sample 50% of the NuSTAR PSF and centered at the optical position of AT 2018cow, we infer a combined count rate upper limit of 1.1×10^{-4} counts s^{-1} (10–79 keV). This translates into a flux limit of $F_{\rm X,hard} < 1.3 \times 10^{-14}$ erg cm^{-2} s^{-1}($L_{\rm X,hard} < 5. \times 10^{39}$ erg s^{-1}) for an assumed spectral power-law index of $\Gamma = 2.9$ that best fits the XMM-Newton data (Obs3; see Section 2).

4. Nature of the Late-time X-Ray Emission

4.1. Transient Emission versus Star Formation

Before proceeding further, we discuss the origin of the late-time X-ray emission, whether it can be ascribed to AT 2018cow, and in what fraction. In nonactive galaxies, like the host of AT 2018cow, a possible source of contamination is represented by the X-ray emission of (i) X-ray binaries (XRBs), both low-mass and high-mass XRBs (LMXRBs and HMXRBs, respectively), which are dominant in the 2–10 keV energy range; and (ii) the hot ISM, mainly relevant below 2 keV. The X-ray luminosities of these components correlate with the star formation rate (SFR; see, e.g., Mineo et al. 2012, 2014; Lehmer et al. 2016, and references therein). We adopted the empirical $L_{\rm X}$–SFR relations in Lehmer et al. (2016), which scale with redshift, SFR, and stellar mass (M_*), and used the SFR and M_* inferred for the host galaxy of AT 2018cow from the SED fitting of the optical data in Perley et al. (2019): ${\rm SFR} = 0.22^{+0.03}_{-0.04}$ $M_\odot$ yr^{-1} and $M_* = (1.42\ ^{+0.17}_{-0.25}) \times 10^9$ $M_\odot$ (also in agreement with Michałowski et al. 2019 and Lyman et al. 2020). We estimated a luminosity range $\sim$(6–9) $\times 10^{38}$ erg s^{-1} for each of the 0.5–2 keV and 2–10 keV bands (similar values are obtained using the relation in Mineo et al. 2014). The estimated 1σ scatter in the relations is 0.17 dex, although the galaxy-to-galaxy spread in the 2–10 keV luminosity could be larger, up to 0.4 dex, and sensitive to variations in metallicity, stellar age, and XRB populations (Lehmer et al. 2016).

The level of the observed emission is thus of the same order as the star formation estimates. However, we note that at $\delta t = 218$ days (Obs3) (i) the emission is significantly brighter than Obs4, thus showing the limitations of the SFR-based inferences; moreover, (ii) the centroid of the X-ray emission is consistent with the position of AT 2018cow (and $6\farcs8$ from the host galaxy core); and (iii) the typical star-forming spectral components (a thermal model with $kT \sim 0.3$–2 keV and a power law with $\Gamma \sim 1.8$–2.0; see, e.g., Lehmer et al. 2016) cannot satisfactorily model the the X-ray spectrum. For Obs4 ($\delta t = 1349-1358$ days), the poor characterization of the X-ray emission in terms of localization and spectral properties makes it difficult to be conclusive between AT 2018cow and a star formation origin. As a further attempt, we used the Chandra observation taken at $\delta t = 8.2$ days (see the Appendix) and calculated the X-ray flux in the host galaxy region (excluding the AT 2018cow emission). Unfortunately, the 90% c.l. upper limit on the 0.3–10 keV unabsorbed flux is 2.4×10^{-13} erg cm^{-2} s^{-1}, corresponding to a 0.3–10 keV luminosity of $\leqslant 10^{41}$ erg s^{-1}, not sufficiently deep to probe the expected star formation luminosities.

In the following we consider two possible scenarios: (i) either the X-ray emission at $\delta t = 1349$–1358 days (Obs4) is still mostly contributed by AT 2018cow, or (ii) AT 2018cow had faded below the detectable level and we are detecting the star-formation-related X-ray emission from the host galaxy. In both cases, the hard X-ray emission from AT 2018cow at this epoch is $L_{\rm X,hard} < 6 \times 10^{39}$ erg s^{-1}(10–79 keV). Furthermore, if scenario (ii) is correct, the star formation component could contribute up to ≈25% of the best-fit X-ray flux measured at $\delta t = 218$ days (Obs3). This raises the question whether the star formation contamination could be responsible for the spectral softening observed in Obs3. Incidentally, we note that a typical star formation X-ray spectrum is not expected to be as soft as the observed one (see, e.g., the template presented in Figure 4 of Lehmer et al. 2016). As a further test, we simulated an X-ray spectrum and supposed the (pessimistic) scenario of a total flux, at the time of Obs3, of 2.8×10^{-15} erg cm^{-2} s^{-1} and a true host flux of 1.4×10^{-15} erg cm^{-2} s^{-1} (both values within $\sim 1\sigma$ of the measured/estimated values), meaning that fully half of the flux detected in Obs3 would be from the host galaxy. For the host galaxy spectrum, we referred to the mean X-ray SED of local star-forming galaxies presented in Lehmer et al. (2016): a thermal model with $kT = 0.5$ keV was assumed for the hot gas and a power law with $\Gamma = 1.9$ for the XRB emission, while the relative contributions were set so that the former (latter) dominates below (above) ∼1.5 keV (see Figure 4 in Lehmer et al. 2016). The X-ray spectrum of AT 2018cow was modeled with a power law with a photon index equal to 1.5, i.e., the value measured at early times. The underlying assumption is that there is no spectral evolution in the X-ray emission of AT 2018cow. Fitting the simulated X-ray spectrum with a composite model that accounts for all contributions, we obtained for AT 2018cow a best-fit photon index $\Gamma = 1.5 \pm 0.7$, while a fit with a simple power-law model corrected for Galactic absorption, as done for Obs3 spectrum, gives a best-fit photon index $\Gamma = 1.8 \pm 0.3$. This is below the observed range measured in Obs3, albeit with large uncertainties, thus supporting the indications of a true spectral softening of the X-ray emission of AT 2018cow.

4.2. AT 2018cow X-Ray Light Curve

The temporal evolution of the soft X-ray flux at the location of AT 2018cow is remarkable: as shown in Figure 2, at $\delta t = 218$ days the 0.3–10 keV $L_{\rm X}$ has dropped by ≈4 orders of magnitude with respect to the time of the discovery (from $\sim 10^{43}$ erg s^{-1} to $\sim 2 \times 10^{39}$ erg s^{-1}). However, between $\delta t = 218$ days and $\delta t = 1349-1358$ days the X-ray flux decreases by a factor $\lesssim$4. We fit the X-ray light curve at $\delta t \leqslant 218$ days with a smoothed broken power-law model, thus assuming that beyond that epoch we are detecting X-ray emission from the host galaxy. The best-fit model (Figure 2) indicates an initial decay $L_{\rm X} \propto t^{-0.59 \pm 0.09}$, which drastically steepens to $L_{\rm X} \propto t^{-4.1 \pm 0.04}$ at $\delta t_{\rm break} \sim 24 \pm 2$ days. Note that this model has the goal to reproduce the long-term evolution of

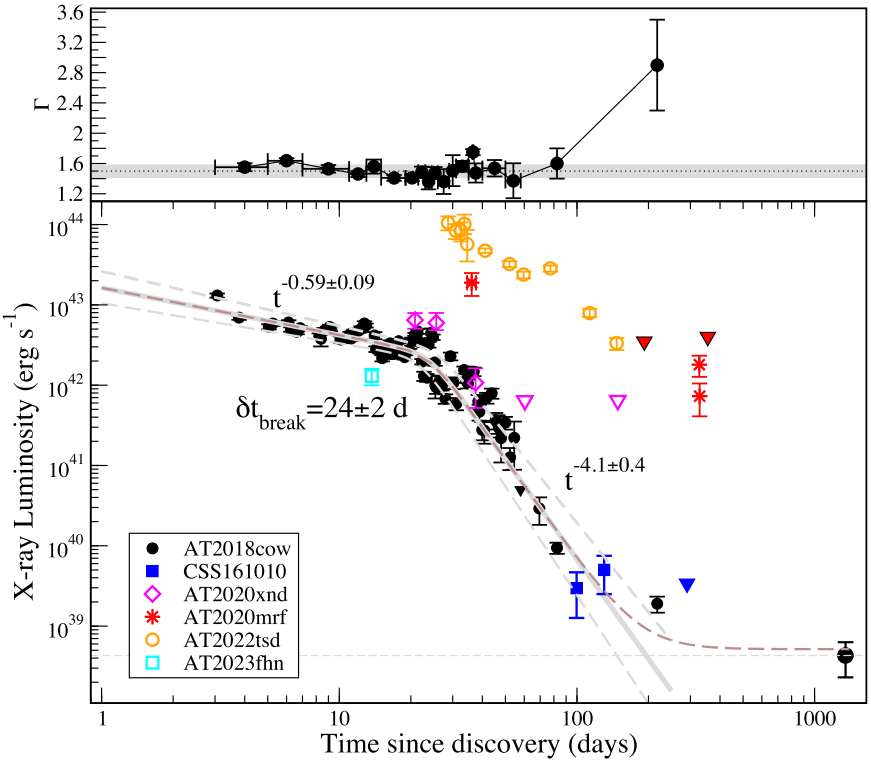

Figure 2. Temporal evolution of AT 2018cow at X-ray energies (0.3–10 keV), as captured by Swift-XRT, XMM-Newton, and Chandra. X-rays are modeled with a power-law spectrum. In the top panel the measured X-ray photon indexes are reported: $\Gamma \sim 1.5$ at early time, while the 218-day spectrum suggests a strong softening, $\Gamma \sim 2.9$. No measurement of Γ was possible for the last XMM observation. The dotted line and gray shaded area are the averaged photon index at $\delta t \lesssim 83$ days and the relative uncertainty. In the bottom panel, the gray solid line is the best-fit broken power-law decay assuming that AT 2018cow has faded after $\delta t \lesssim 218$ days, the short-dashed gray lines being the uncertainties on the model parameters. The long-dashed brown line is the broken power law with the addition of a constant component, mimicking a late-time flattening of the light curve, under the hypothesis that the X-ray flux at $\delta t = 1349-1358$ days is associated with AT 2018cow (see text). The five X-ray-detected FBOTs, CSS 161010 (Coppejans et al. 2022), AT 2020xnd (Ho et al. 2022a; Bright et al. 2022), AT 2020mrf (Yao et al. 2022), AT 2022tsd (Matthews et al. 2023), and AT 2023fhn (Chrimes et al. 2024), are also shown for comparison.

the X-ray emission, not the superposed hour-to-day temporal variability, evident from the residuals, which was discussed in previous works (Rivera Sandoval et al. 2018; Margutti et al. 2019). As the spectrum softens, the observed L_X at $\delta t = 218$ days appears in excess ($\sim 2.7\sigma$) with respect to the broken power-law model. In the hypothesis that the emission is instead still associated with AT 2018cow, a new component, here chosen to be constant with $L_X = 4 \times 10^{38}$ erg s^{-1}, needs to be added to the X-ray light-curve model (smoothed broken power law+constant) to match the last XMM-Newton epoch. We will discuss the implications of a persistent versus rapidly fading X-ray emission in FBOTs at $\delta t \gtrsim 100$ days in Section 6.

5. Late-time Broadband Radio–UV–X-Ray SEDs

AT 2018cow was observed with the the Karl G. Jansky Very Large Array (VLA) at $\delta t = 82$–328 days (PI Coppejans; Ho et al. 2019; Margutti et al. 2019; D. L. Coppejans et al., 2024, in preparation), with the Giant Metrewave Radio Telescope (GMRT) extending to $\delta t = 570$ days (PI Nayana; Nayana & Chandra 2021) and with HST in the time window $\delta t = 50$–1475 days (PIs Y. Chen, A. Filippenko, R. Foley, M. Drout, A. Levan; Sun et al. 2022; Chen et al. 2023a, 2023b; Inkenhaag et al. 2023; Sun et al. 2023). In the following we model the multiwavelength data sets that are approximately coeval with XMM-Newton Obs3 and Obs4.

Multifrequency radio observations were performed at $\delta t = 217$–221 days (VLA, 1.5–33 GHz; D. L. Coppejans et al. 2024, in preparation) and $\delta t = 227$–234 days (GMRT, at 0.4, 0.75 and 1.25 GHz; Nayana & Chandra 2021), thus coeval with XMM-Newton Obs3. The radio-to-X-ray SED is shown in Figure 3. We fit the radio F_ν data with a smoothed broken power-law model of the form

$$F_\nu(\nu) = F_{\rm pk}\left[\left(\frac{\nu}{\nu_b}\right)^{-\alpha_{r,1}/s} + \left(\frac{\nu}{\nu_b}\right)^{-\alpha_{r,2}/s}\right]^{-s}, \quad (1)$$

which is typical of the synchrotron emission originating from the deceleration of astrophysical outflows associated with TDEs or SNe (e.g., Chevalier & Fransson 2017). We find a best-fitting break frequency $\nu_b = 4.2 \pm 0.7$ GHz, peak flux density of $F_{\rm pk} = 2.4 \pm 1.4$ mJy, optically thick slope $\alpha_{r,1} = -2.0 \pm 0.3$, and optically thin slope $\alpha_{r,2} = 0.7 \pm 0.3$ (with a smoothing parameter $s = 1.4 \pm 0.9$). The VLA data will be discussed in detail elsewhere. Here it is sufficient to note that the extrapolation of the radio to the X-ray band severely underpredicts the X-ray flux, confirming that the emission in the two energy bands is produced by two distinct components, as found for the previous epochs (Margutti et al. 2019). Specifically, the shock–CSM interaction power that explains the radio data cannot account for the bright X-ray (and UV; see Figure 3) emission from AT 2018cow.

Late-time multiband UV photometry was acquired with HST at $\delta t = 714$–1136 days and $\delta t = 1475$ days (Figure 2). The analysis of these observations has been presented in Sun et al. (2022, 2023), Chen et al. (2023a, 2023b), and Inkenhaag et al.

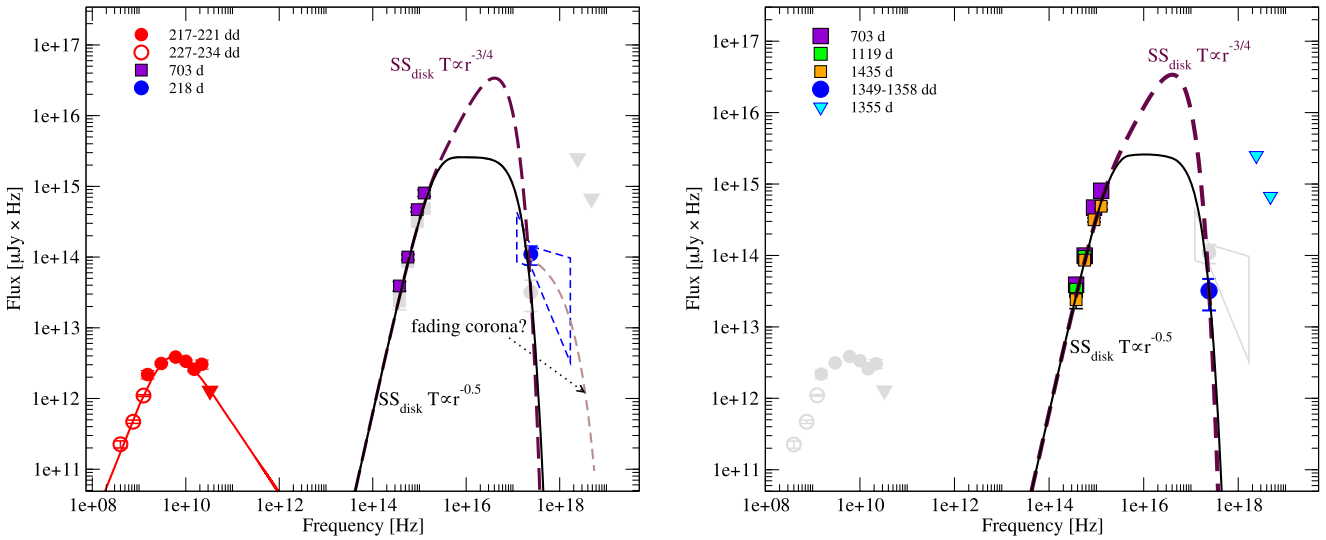

Figure 3. Left panel: AT 2018cow radio-to-X-ray SED at $\delta t \sim 217$–234 days. The red solid line is the best-fit broken power-law model for the radio data (GMRT and VLA from Nayana & Chandra 2021 and D. L. Coppejans et al. 2024, in preparation, respectively). The bow tie is the best-fit power-law model ($\Gamma \sim 2.9$) from the X-ray spectral analysis of Obs3. Gray points are data taken at $\delta t \sim 1100$–1440 days. Right panel: optical/UV-to-X-ray SED at $\delta t \sim 700$–1440 days. While for the modeling we formally associate the X-ray flux of Obs4 with AT 2018cow, this assumption is relaxed in the discussion on the nature of the accretor (see the text). The optical/UV fluxes (colored squares) are the HST data from Chen et al. (2023a, 2023b). Triangles are NuSTAR data. Gray points are data acquired at $\delta t \sim 217$–234 days. In both panels, the long-dashed line is a standard Shakura–Sunyaev ($T \propto r^{-3/4}$) disk modeling the HST and soft X-rays (blue circle) at $\delta t \sim 1350$–1435 days, while the thin black line assumes a disk temperature evolution as $T \propto r^{-1/2}$ (i.e., Shakura & Sunyaev 1973 "windy" solution, or disks where radiation is trapped within the inflow and advected onto the accretor). In addition, at $\delta t \sim 220$ days, we added a power law ($\Gamma \sim 2.0$) with an exponential cutoff at $\approx$3 keV, mimicking a fading Comptonized component.

(2023). These studies agree on the presence of a luminous ($L_{\rm UV} \gtrsim 10^{39}$ erg s^{-1}), blue ($T_{\rm eff} \gtrsim 10^{4.6}$ K), and persistent (albeit slowly fading) UV source at the location of AT 2018cow.[23] The UV spectrum is consistent with the $F_\nu \propto \nu^2$ expected for the Rayleigh–Jeans tail of an optically thick thermal spectrum. Chen et al. (2023a) find indications of a chromatic flux decay, with a flattening of the near-UV spectrum in the last HST epoch, possibly pointing at cooling and expansion of the emitting region. The (slow) decay of the UV emission is not consistent with a stellar origin and suggests instead a physical association with AT 2018cow. Interestingly, similarly luminous, hot, and lingering UV emission has been detected in TDEs in the lower BH mass bin (i.e., $M_\bullet \lesssim 10^{6.5}\,M_\odot$) years after the optical flare (van Velzen et al. 2019; Mummery et al. 2024), and the similarity of the UV behavior of AT 2018cow and TDEs (and its astrophysical implications) has been recently pointed out by Inkenhaag et al. (2023).

HST data at $\delta t = 1475$ days are approximately coeval with XMM-Newton Obs4 and NuSTAR data.[24] Given the soft X-ray spectrum and the similar temporal behavior, we consider the possibility that the optical/UV emission and X-ray emission belong to the same radiative component, which we first model with the standard Shakura & Sunyaev (1973) multicolor blackbody thin disk with a radial temperature scaling $T(r) \propto r^{-3/4}$ (solid line in Figure 3). The best-fitting parameters are an inner disk temperature $T_{\rm in} \sim 10^{5.91\pm0.02}$ K (which is $\approx$0.06 keV), outer disk temperature $T_{\rm out} \sim 10^{4.45\pm0.18}$ K, and inner disk radius $R_{\rm in} \sim 10^{10.3\pm0.1}$ cm, which corresponds to the innermost stable circular orbit (ISCO) of a nonrotating BH with mass $M_\bullet \sim 2.4 \times 10^4\,M_\odot$ ($R_{\rm ISCO} = 6R_g$, and the gravitational radius is $R_g \equiv GM_\bullet/c^2 \approx 1.5 \times 10^6 (M_\bullet/10\ \ M_\odot)$ cm). These parameters imply an outer disk radius $R_{\rm out} \approx 37\,R_\odot$ from which most of the UV radiation is generated and a BH accretion rate well below the Eddington limit $\dot{M}_\bullet \approx 0.01 \dot{M}_{\rm Edd}$, where we follow the convention $\dot{M}_{\rm Edd} \equiv L_{\rm Edd}/0.1\,c^2$. Less steep disk temperature profiles $T(r) \propto r^{-\alpha}$ with $\alpha < 3/4$ such as those expected when radial flux advection is important (e.g., Narayan & McClintock 2008) lead to similar inferences on $T_{\rm in}$, $T_{\rm out}$, and $\dot{M}/\dot{M}_{\rm Edd}$ but smaller accretor masses $10^3\,M_\odot \lesssim M_\bullet \lesssim 10^4 M_\odot$ (Figure 3).

The inferred low temperature $T_{\rm in} \sim T_{\rm X}$ of the inner disk, set to truncate at the ISCO, is what drives the inference of IMBH-like accretor masses accreting at sub-Eddington rates (a similar argument motivated IMBH models for ultraluminous X-ray sources (ULXs); e.g., Miller et al. 2004b, 2004a; King et al. 2023). For $\dot{M}_\bullet \lesssim \dot{M}_{\rm Edd}$, the disk will be a standard thin disk (e.g., Frank et al. 2002), for which the effective temperature of the radiation from the innermost radii is approximately given by

$$kT_{\rm X} \approx k\left(\frac{3GM_\bullet\dot{M}}{8\pi\sigma R_{\rm ISCO}^3}\right)^{1/4} \simeq$$
$$0.1\ {\rm keV}\left(\frac{\dot{M}_\bullet}{0.01\,\dot{M}_{\rm Edd}}\right)^{1/4}\left(\frac{M_\bullet}{10^4\,M_\odot}\right)^{-1/4}\left(\frac{R_{\rm ISCO}}{4R_g}\right)^{-3/4}. \quad (2)$$

Within this set of models, from Equation (2), smaller accretors with $M_\bullet \sim 10$–$100\,M_\odot$ are coupled with inner disks that are hotter than (and not consistent with) the observed X-rays. We note that this argument is independent of the detected X-rays being physically associated with AT 2018cow or instead just providing a limit on the emission from

[23] In the following analysis we adopt the HST photometry values presented in Chen et al. (2023a, 2023b). However, we note that consistent findings would be obtained by using the photometry presented in the other studies, without any significant impact on our major conclusions.

[24] Based on the very slow evolution of the source at these epochs in both the UV and X-rays, we do not expect that the difference of $\Delta t \sim 100$ days between the acquisition time of these data sets will impact our major conclusions.

AT 2018cow. Mathematically, this is a consequence of $\nu F_\nu|_{\rm UV} > \nu F_\nu|_{\rm X}$. For the same reason, our inferences are consistent with those of Chen et al. (2023a), where the authors used a shallower X-ray limit from Swift-XRT observations to reach a similar conclusion. However, differently from previous studies, we argue that these geometrically thin disk models cannot be used to rule out $M_\bullet \sim 10$–$100\,M_\odot$ BH accretors, as in that case super-Eddington mass supplies $\dot{M}_\bullet \gg \dot{M}_{\rm Edd}$ are needed, which causes strong deviations from the geometrically thin disk picture since $H/R \sim L(R)/L_{\rm Edd}$, where H and R are the disk height and radius, respectively (e.g., Frank et al. 2002). We discuss models of supercritical accretion that might apply to LFBOTs in Section 6.

In this scenario, the disk is supposed to be present also at earlier times. Modeling of the optical/UV to X-ray emission at $\delta t = 217$–703 days provides us with parameter values consistent with those of the last epoch, with the caveat that the optical/UV flux at the time of Obs3 could have been higher. Interestingly, this model leaves an excess in the X-ray spectrum of Obs3, as supported by the X-ray spectral fit of a blackbody model resulting in a higher temperature and lower normalization (see Section 2.2). One possibility is that at $\delta t = 218$ days we are still detecting the nonthermal component, which was dominant at early times and is now rapidly fading (see Figure 3) and possibly driving the fast decay of the X-ray light curve at $\delta t > 24$ days.

6. Discussion

Deep late-time XMM-Newton observations out to $\delta t \approx 1360$ days revealed a distinctive temporal and spectral evolution (Figure 2) of the X-ray emission from the direction consistent with AT 2018cow. Additionally, the last two XMM-Newton observations of AT 2018cow at $\delta t > 200$ days indicate a spectral change from a relatively hard to a very soft spectrum. Given that most of the X-ray photons are detected at very soft X-ray energies, obscuration is unlikely. We note that the lack of an intrinsic absorber is in line with observations at early times (Section 2).

We discuss the implications of a soft X-ray source of emission in an LFBOT and its connection with the luminous, declining UV source, reported by Sun et al. (2023) and Chen et al. (2023a), within the context of the shock interaction model (Section 6.1) and accretion-powered emission on a compact object (Section 6.2). In the following, we assume that the association of the X-ray emission with AT 2018cow is robust for Obs3. Our main arguments hold true independently from the soft X-ray source of Obs4 being physically associated with AT 2018cow or regarded as a limit.

6.1. Shock Interaction with the Medium

The SED of AT 2018cow at ∼220 days clearly shows that the emission in the radio and X-ray bands stems from two separate radiative components and that the X-ray emission is in clear excess to the extrapolation of the synchrotron spectrum that best fits the shock-interaction-powered radio emission of AT 2018cow (Figure 2, bottom panel). However, for shocks that propagate within regions of CSM with high densities, the X-ray emission is expected to be dominated by thermal bremsstrahlung radiation (e.g., Fransson et al. 1996; Chevalier & Fransson 2017), as was observationally confirmed in SN 2014C (Margutti et al. 2017; Brethauer et al. 2022; Thomas et al. 2022). In this scenario, and assuming electron–ion equipartition, the temperature of the emission T is related to the shock velocity as $T \approx 2.27 \times 10^9 \mu_p v_4^2$ K, where v_4 is the shock velocity in units of 10^4 km s^{-1}, $\mu_p \approx 0.6$ is the mean mass per particle including protons and electrons, and we assumed solar composition and complete ionization, which is appropriate for a forward-shock-powered X-ray emission.[25] The observed very soft spectrum implies $k_b T \ll 0.2$ keV or $v \ll 250$ km s^{-1}, which is in stark contrast with the $v \sim 0.2c$ derived from the radio modeling at 257 days (Nayana & Chandra 2021). We conclude that the forward shock that is powering the radio emission cannot be the source of energy behind the persistent, soft X-ray emission. A similar conclusion is supported by the independent analysis of the late-time UV emission (Chen et al. 2023a), which we do not replicate here.

6.2. Accretion-powered Scenarios for AT 2018cow and LFBOTs

In this section we explore scenarios that connect the observed late-time UV to X-rays with manifestation of accretion processes onto a compact object. We start by summarizing the inferences from the early-time data at $\delta t < 200$ days that are relevant here and independently support this physical scenario.

Generically, Compton hump spectra like those observed in AT 2018cow (Margutti et al. 2019, their Figure 6) have been observationally associated with accreting sources like those of active galactic nuclei (AGN) or XRBs; see, e.g., Reynolds (1999), Risaliti et al. (2013), and Belloni & Motta (2016). More specifically, the following apply: (i) The observed X-ray and UV emission from AT 2018cow reaching $L_{\rm X+UV} \approx 5 \times 10^{44}$ erg s^{-1}, if accretion powered, implies a super-Eddington regime for any accretor with mass $\leqslant 10^6\,M_\odot$. Borrowing the argument from the ULX literature (e.g., King et al. 2023), this large luminosity, if disk powered, requires beaming of the emission even for super-Eddington mass supplies. (ii) This supercritical accretion scenario is independently supported by the significantly blueshifted Fe Kα fluorescent line observed in AT 2018cow at $\delta t \leqslant 8$ days (Margutti et al. 2019). The numerical simulations by Thomsen et al. (2019), which were originally motivated by the discovery of such a strongly blueshifted Fe Kα line in the jetted relativistic TDE Swift J1644 (Kara et al. 2016), showed that hot (6.7–6.97 keV rest-frame), strongly blueshifted (≈8 keV centroid) Fe Kα fluorescent lines are a robust observational signature of super-Eddington accretion disks irradiated by a lamp-post corona. Optically thick outflows are launched from the super-Eddington disk and create a conical funnel structure that provides the reflecting surface shaping the line profile, in close similarity to the model invoked by Margutti et al. (2019). Note that at $\delta t = 218$ days we could still be detecting the rapidly cooling corona emission. (iii) The outflow velocity required to produce the observed Fe Kα line shift is $v \approx 0.2c$, which is similar to the inferred velocity of the optical photosphere of AT 2018cow at early times and to the velocity of its radio-emitting material (Ho et al. 2019; Margutti et al. 2019; Nayana & Chandra 2021).

These velocities are significantly larger than thermal (or magnetocentrifugal) winds from sub-Eddington XRBs but

[25] For shocked SN ejecta chemical composition and complete ionization, which is appropriate for a reverse-shock-powered X-ray emission, $\mu_p \approx 1.33$.

intriguingly similar to the velocity of ≈ a few $0.1c$ expected to be associated with outflows launched by super-Eddington accretion disks (e.g., Thomsen et al. 2019 and references therein).[26]

6.2.1. Inner Accretion Disk Temperature: IMBHs versus $M_\bullet \sim 10$–$100\,M_\odot$ BHs

The inferences above support a physical connection between the early emission from AT 2018cow and the manifestation of a super-Eddington accretion phase (like in jetted TDEs, GRBs, and ULXs) independently from the accretor mass. From an X-ray perspective, the X-ray constraints at $\delta t \gtrsim 200$ days indicate that the system evolves from a luminous, spectrally hard, and super-Eddington regime to a remarkably fainter, softer, and ⩽Eddington one (Figure 2). We thus consider that one of three potential transient events (i.e., a massive stellar core collapse, Wolf–Rayet BH merger, IMBH-TDE) results in the formation of a (super-Eddington) accretion disk of initial outer radius $R_{d,0}$ around a BH of mass $M_\bullet$. The disk spreads with time as $R_d(t)$ and evolves to an innermost ring temperature T_X by the time of our X-ray observations.

For $\dot{M}_\bullet \lesssim \dot{M}_{\rm Edd} \equiv L_{\rm Edd}/(0.1c^2)$, the disk will be a standard thin disk, for which the effective temperature of the radiation from the innermost radii is approximately given by Equation (2). However, for $\dot{M}_\bullet \gg \dot{M}_{\rm Edd}$ we expect powerful outflows from the inner regions of the disk (e.g., Narayan & Yi 1995; Blandford & Begelman 1999; Kitaki et al. 2021), which can carry a substantial fraction of accreted matter and can place the photosphere radius at radii $\gg R_{\rm ISCO}$. In particular, a steady quasi-spherical wind with a mass-loss rate $\dot{M}_w \sim \dot{M}_\bullet$ and velocity $v_w \sim c$ launched from $\sim R_{\rm ISCO}$ will possess a density profile at radii $r \gg R_{\rm ISCO}$ given by $\rho_w = \frac{\dot{M}_w}{4\pi r^2 v_w}$. The optical depth of the wind above a radius r is

$$\tau_w = \int_r^\infty \rho_w \kappa dr = \frac{\dot{M}_w \kappa}{4\pi r v_w}, \tag{3}$$

such that the photosphere radius ($\tau_w = 1$) is

$$r_{\rm ph} = \frac{\kappa \dot{M}_w}{4\pi v_w} = 10 R_g \left(\frac{\dot{M}_w}{\dot{M}_\bullet}\right)\left(\frac{\dot{M}_\bullet}{\dot{M}_{\rm Edd}}\right)\left(\frac{v_w}{c}\right)^{-1}, \tag{4}$$

where we take an electron-scattering-dominated opacity (for fully ionized gas with H-dominated composition) $\kappa \approx \sigma_T/m_p \approx 0.38$ cm^2 g^{-1}, σ_T and m_p being the Thompson cross section and the proton mass, respectively. Assuming that the emitted luminosity follows $L_X \simeq \eta \dot{M}_\bullet c^2$ with radiative efficiency $\eta \sim 0.03$ as predicted by simulations of super-Eddington accretion (e.g., Sadowski & Narayan 2016), this predicts a maximum emission temperature for thermal emission from the innermost radii of the disk given by

$$kT_X \approx \left(\frac{L_X}{4\pi\sigma r_{\rm ph}^2}\right)^{1/4}$$
$$\approx 0.85\ {\rm keV}\ \eta_{-1}^{1/4}\left(\frac{M_\bullet}{10\,M_\odot}\right)^{-1/4}\left(\frac{\dot{M}_\bullet}{\dot{M}_{\rm Edd}}\right)^{-1/4}\left(\frac{v_w}{c}\right)^{-1/2}, \tag{5}$$

where $\eta_{-1} \equiv \eta/(0.1)$; we have taken $\dot{M}_w \sim \dot{M}_\bullet$ as expected for super-Eddington accretion disks that lose an order-unity fraction of their inflowing mass across each decade of radius (e.g., Blandford & Begelman 1999), and we used $L_X = \eta \dot{M}_\bullet c^2$.

Unlike a thin disk for which T_X increases for higher accretion rate (Equation (2)), for super-Eddington accretion the thermal photosphere temperature decreases for higher accretion rate.[27] For example, if $M_\bullet = 100\,M_\odot$, $\dot{M}_\bullet \sim 10\dot{M}_{\rm Edd}$, and $\eta \sim 0.01$, Equation (5) gives $kT_X \approx 0.15$ keV, similar to the thin-disk temperature (Equation (2)) for a higher-mass IMBH $M_\bullet \sim 10^4 M_\odot$ accreting at $\dot{M}_\bullet \ll \dot{M}_{\rm Edd}$, corresponding to $L_X \sim 10^{39}$ erg s^{-1} (similar to our last observations of AT 2018cow; Figure 2). Stated another way, for any observed L_X and T_X, there can be two allowed solutions: sub-Eddington for a high-mass (i.e., IMBH-like) BH (Equation (2)), and super-Eddington for a low-mass BH (Equation(5)). This argument applies independently of the physical association of the late-time soft X-ray source to AT 2018cow.

6.2.2. Outer Accretion Disk Radius: IMBHs versus $M_\bullet \sim 10$–$100\,M_\odot$ BHs

Late-time UV observations of AT 2018cow constrain the outer disk radius at $\delta t \approx 1500$ days to a value $R_d \approx 40\,R_\odot$ (Section 5). In this section we discuss the expectations from accretion disks formed by a core-collapse stellar explosion, an IMBH-TDE, and a Wolf–Rayet (W–R) BH merger.

In the core-collapse case, the initial disk radius $R_{d,0}$ depends on the angular momentum of the progenitor star but—insofar that angular momentum is at a premium (e.g., Fuller & Ma 2019)—is typically expected to be just outside the ISCO radius of at most tens of gravitational radii $R_g \equiv GM_\bullet/c^2 \approx 1.5 \times 10^6 (M_\bullet/10\ M_\odot)$ cm. Hence, we expect $R_{d,0} \lesssim 10^7$ cm in the core-collapse case.

In the IMBH-TDE case, the characteristic disk radius is at most (i.e., for a typical $\beta \simeq 1$ encounter, where $\beta \equiv R_t/R_p$ is the penetration parameter, with R_p the periapse) equal to twice the tidal radius R_t:

$$R_{d,0} \simeq 2R_t \simeq 2R_\star \left(\frac{M_\bullet}{M_\star}\right)^{1/3}$$
$$\approx 3 \times 10^{12}\ {\rm cm} \left(\frac{R_\star}{R_\odot}\right)\left(\frac{M_\star}{M_\odot}\right)^{-1/3}\left(\frac{M_\bullet}{10^4\,M_\odot}\right)^{1/3}, \tag{6}$$

where $M_\star$ and $R_\star$ are the mass and radius of the disrupted star, respectively, and we have normalized $M_\bullet$ to $10^4\ M_\odot$ to match the fall-back time of the debris $t_{\rm fb} \simeq 5.8\ {\rm days} (M_\bullet/10^4\ M_\odot)^{1/2}$ (e.g., Stone et al. 2013) with the AT 2018cow peak engine duration ∼optical rise time $t_{\rm rise} \sim 3$ days.

The disruption process setting the disk size in the W–R merger case is similar to the TDE scenario, except the BH is much less massive ($M_\bullet \sim 10$–$100\,M_\odot$) and the mass of the WR star ($M_\star \sim 10\,M_\odot$) is generally greater than that of the Sun, resulting in $R_{d,0} \sim R_\odot \sim 10^{11}$ cm (e.g., Metzger 2022).

[26] Consistently, these "ultrafast outflows" have been located in several ULXs; see, e.g., King et al. (2023) for a recent review.

[27] However, we note that nonthermal X-ray emission such as that observed at early times in AT 2018cow can originate above the photosphere and will not follow Equation (5).

After forming, the disk will begin to accrete on the viscous timescale

$$t_{\rm visc,0} \sim \left.\frac{r^2}{\nu}\right|_{R_{d,0}} \approx 5.0 \text{ days } \alpha_{-2}^{-1}\left(\frac{R_{d,0}}{R_\odot}\right)^{3/2}\left(\frac{M_\bullet}{10\,M_\odot}\right)^{-1/2}\left(\frac{H/r}{1/3}\right)^{-2}, \quad (7)$$

where $\nu = \alpha c_s H = \alpha r^2 \Omega_K (H/r)^2$ is the effective kinematic viscosity, $\Omega_K = (GM_\bullet/r^3)^{1/2}$, $\alpha = 10^{-2}\alpha_{-2}$, c_s is the sound speed, and we have normalized the equation to the case of a geometrically thick disk with $H/r \sim 1/3$ (see below). In the W–R BH merger case, the LFBOT engine timescale $\lesssim$3 days (for $\alpha \sim 0.01$–0.1) is naturally set by $t_{\rm visc,0}$. However, in the core-collapse case $R_{d,0} \ll R_\odot$, and as a result $t_{\rm visc,0}$ is too short to represent the engine activity timescale of AT 2018cow, which would instead be set by the freefall time of the infalling stellar envelope. The viscous time in the IMBH-TDE case can also (just barely) obey $t_{\rm visc,0} \lesssim t_{\rm rise}$ for high α and/or small stellar radius $R_\star \lesssim R_\odot$.

On timescales $t \gtrsim t_{\rm visc,0}$, the disk will establish a steady flow onto the central compact object. Taking $M_{d,0} \sim M_\star \sim 1$–$10\,M_\odot$ as the mass of the disk, the peak accretion rate near the outer disk edge $\sim R_{d,0}$ can be estimated as

$$\dot{M}_0 \sim \frac{M_{d,0}}{t_{\rm visc,0}} \sim 10^{28} \text{g s}^{-1}\left(\frac{M_{d,0}}{M_\odot}\right)\left(\frac{t_{\rm visc,0}}{3 \text{ days}}\right)^{-1}. \quad (8)$$

This is $\gtrsim$6–10 orders of magnitude larger than the Eddington rate $\dot{M}_{\rm Edd} \equiv L_{\rm Edd}/(0.1c^2) \sim (M_\bullet/10\,M_\odot)10^{19}$ g s^{-1}, justifying our assumption of a geometrically thick disk with $H/r \sim 1/3$ (e.g., Sadowski & Narayan 2015).

For the high mass inflow rates $\dot{M} \gg \dot{M}_{\rm trap} \equiv 10\,\dot{M}_{\rm Edd}(R_{d,0}/R_g) \sim 10^4 \dot{M}_{\rm Edd}$ of interest, photons are trapped and advected inward through the disk at radii $\lesssim R_{d,0}$ (e.g., Begelman 1979). Since the disk cannot cool efficiently via radiation (e.g., Shakura & Sunyaev 1973), the accretion flow in this "hyperaccretion" regime is susceptible to outflows powered by the released gravitational energy (e.g., Narayan & Yi 1995; Blandford & Begelman 1999; Kitaki et al. 2021). These outflows are responsible for creating the conical funnel geometry where the blueshifted Fe Kα line is formed and provide a natural explanation for the AT 2018cow fastest ejecta traced by radio observations (Section 6.2). Such outflows cause the mass inflow rate $\dot{M}$ to decrease approaching the BH surface, in a way typically parameterized as a power law in radius,

$$\dot{M}(r) \approx \dot{M}_0\left(\frac{r}{R_{d,0}}\right)^p, \quad (9)$$

where values for the parameter $p \approx 0.6$ are motivated by numerical simulations of radiatively inefficient accretion flows (e.g., Yuan & Narayan 2014).

At late times $t \gg t_{\rm visc,0}$, the outer edge of the disk will spread outward from its initial radius $R_{d,0}$ owing to the redistribution of angular momentum:

$$R_d(t) \simeq R_{d,0}\left(\frac{t}{t_{\rm visc,0}}\right)^m, \quad t \gg t_{\rm visc,0}, \quad (10)$$

where the parameter m depends on the properties of the disk outflows. If the disk outflows carry away only the local specific angular momentum of the disk material, then the outer edge of the disk will grow with time as $m = 2/3$ (e.g., Cannizzo et al. 1990). However, in the case of a net torque on the disk, one can instead have $m = 1/(1.5+p) \simeq 0.48$ (Metzger et al. 2008), where in the final equality we take $p = 0.6$.

Thus, by the time of the HST observations $\delta t \sim 1500$ days, the disk will spread to a radius $R_{1500\rm d} \gtrsim (1500 \text{ days}/t_{\rm visc,0})^m R_{d,0} \sim (15$–$40)R_{d,0}$, where we demand $t_{\rm visc,0} \lesssim 3$ days to match the maximum initial rise time of AT 2018cow. Thus, we predict $R_{1500\rm d} \sim 15$–$40\,R_\odot$ for the W–R BH merger case, in overall agreement with the inferences from the late-time HST observations of AT 2018cow, but generally significantly larger or smaller values in the IMBH-TDE or core-collapse cases, respectively. From this perspective, the W–R BH merger scenario provides a natural explanation of the inferred size of the accretion disk at late times, while the other two scenarios struggle to explain the size of the UV-emitting region. We note that a potentially viable option is represented by the IMBH tidal disruption of a very small star with $R_\star \approx 0.1\,R_\odot$ and $M_\star \approx 0.1\,M_\odot$.

We end with a note on the expected evolution of the accretion power in the W–R BH merger and IMBH-TDE models. The accretion rate at disk radii $r < R_d$ will drop as a power law in time (e.g., Metzger et al. 2008), viz.,

$$\dot{M} \propto r^p t^{-4(p+1)/3}, \quad t \gg t_{\rm visc,0}, \quad (11)$$

such that the accretion rate reaching the central BH will decay as

$$\dot{M}_\bullet \sim \dot{M}_0\left(\frac{R_g}{R_{d,0}}\right)^p\left(\frac{t}{t_{\rm visc,0}}\right)^{-\frac{4(p+1)}{3}}, \quad (12)$$

for $t \gg t_{\rm visc,0}$. This results in a jetted accretion power

$$L_{\rm acc} \sim \eta \dot{M}_\bullet c^2 \approx \approx 10^{45}\eta_{-2}\left(\frac{M_\bullet}{100\,M_\odot}\right)^{0.4}\left(\frac{M_{d,0}}{10\,M_\odot}\right)\left(\frac{M_\star}{10\,M_\odot}\right)^{0.2} \times \times\left(\frac{R_\star}{1\,R_\odot}\right)^{-0.6}\left(\frac{t_{\rm visc,0}}{3 \text{ days}}\right)^{1.1}\left(\frac{t}{3 \text{ days}}\right)^{-2.1} \text{erg s}^{-1}, \quad (13)$$

where we have used Equations (6), (8), and (12) for $p = 0.6$. This expression is valid for $t \gtrsim t_{\rm visc,0}$. We observe that $L_{\rm acc}$ is broadly similar in normalization and power-law decay rate $L_{\rm acc} \propto t^{-2.1}$ to the optical/UV light curve of AT 2018cow (e.g., Margutti et al. 2019, their Figure 9; Chen et al. 2023a), suggesting that the early UV/optical emission from AT 2018cow might also be powered by accretion processes onto a BH.

6.3. Comparison with Other LFBOTs: A Unifying Model

The long-term evolution of the X-ray emission from the location of AT 2018cow is characterized by three regimes: (i) an initial, highly luminous, slowly decreasing phase at $\delta t \lesssim 24$ days with fast temporal variability superimposed; (ii) a rapid decay (a drop of about three orders of magnitude in $\sim$200 days); possibly followed by (iii) a late-time flattening phase with $L_X \sim 4 \times 10^{38}$ erg s^{-1} at $\delta t \gtrsim 200$ days with a soft X-ray spectrum, which, however, might be contaminated, or

even dominated, by the host emission. The presence of luminous, lingering optical/UV emission during phase (iii) (Sun et al. 2022; Chen et al. 2023a, 2023b; Sun et al. 2023), which is reminiscent of TDEs in the lowest mass bin (van Velzen et al. 2019; Inkenhaag et al. 2023; Mummery et al. 2024), indirectly supports the physical association of the persistent, soft X-ray emission with AT 2018cow. Indeed, a further deep X-ray observation, able to probe the flux level measured in Obs4, could help to better discriminate the AT 2018cow contribution from the host galaxy one.

The other five X-ray-detected LFBOTs showed an X-ray luminosity comparable to or larger than AT 2018cow (Figure 2), with AT 2022tsd rivaling the brightest LGRB ever detected (Matthews et al. 2023). In the accretion-reprocessing scenario, more luminous X-ray emission can be a consequence of more powerful accretion and/or more favorable geometry (i.e., a pole-on viewing angle; Metzger 2022), so that brighter or dimmer X-rays detected for other LFBOTs might be a consequence of the geometry of the emission and the location of the observer with respect to the pole.[28] Since Fe Kα fluorescent lines are visible only to nonequatorial observers (i.e., for observers at large angles from the poles the Fe Kα emission is hidden by the optically thick disk and wind), it is plausible that the other LFBOTs with luminous X-rays also had transient Fe Kα spectroscopic features (and Compton humps) that were missed because their X-ray monitoring started too late (Figure 2). As a reference, the Fe Kα line subsided at $\delta t > 10$ days in AT 2018cow, and no other LFBOT has X-ray observations at these early epochs. Similarly, the large distances of all other LFBOTs prevent meaningful constraints on the presence of faint persistent X-ray emission at late time $\delta t > 200$ days. Therefore, other LFBOTs need to be discovered in the local universe (i.e., within $d \lesssim 50$ Mpc) and at very early stages of their evolution (i.e., within days), in order to assess the occurrence of the Fe Kα line complex (and the associated Compton hump feature) and validate the late-time soft X-ray flattening.

We end by noting that this LFBOT unification model, where the optical/UV and X-ray emission is powered by accretion (in the super-Eddington regime at early times, decreasing to $\leqslant$Eddington at late times) and the radio emission is powered by the deceleration of the outflows into the CSM, naturally predicts the presence of AT 2018cow–like transients that are viewed edge-on and will thus appear X-ray dim *if* their optical/UV emission is detectable by these "equatorial" observers.

7. Summary and Conclusions

We presented the first deep X-ray observations of an LFBOT at $\sim$3.7 yr after optical discovery. These observations sampled a pristine portion of the observational phase space of FBOTs and revealed the presence of a luminous, persistent, soft X-ray source of emission at the location of AT 2018cow. The association with AT 2018cow of such emission appears robust at $\delta t \sim 220$ and uncertain at $\delta t \sim 1350$ days, given the potentially comparable level of the X-ray flux from the host galaxy. We modeled the soft X-ray emission in the broader context of the late-time panchromatic observations of AT 2018cow, which includes luminous and slowly fading UV emission that is reminiscent of that detected from TDEs in the lowest mass bin years after the stellar disruption, as recently pointed out by Inkenhaag et al. (2023). We find that these late-time panchromatic observations of AT 2018cow are consistent with either sub-Eddington accretion on an IMBH ($M_\bullet \approx 10^3$–$10^4\,M_\odot$) or the manifestation of $\sim$Eddington-like accretion processes on a lower-mass accretor, e.g., a BH of $M_\bullet \approx 10$–$100\,M_\odot$. While similar arguments have been used in the ULX literature based on the detection of soft X-rays from these systems,[29] we note that this conclusion is independent of the physical association of the soft X-ray source with AT 2018cow (i.e., the argument applies even if we interpret the soft X-ray emission as a limit on the X-ray luminosity output of AT 2018cow at these late epochs).

Assuming that the UV emission originates from the outermost annuli of a spreading disk, we showed that, with the exception of very small stars, the IMBH-TDE model ($M_\bullet \approx 10^3$–$10^4\,M_\odot$) struggles to explain the inferred accretion disk radius, in addition to lacking a natural explanation for the dense CSM with a steep cutoff at $r \sim$ a few $\times\ 10^{16}$ cm implied by the analysis of the radio observations of AT 2018cow and other LFBOTs. The detection of an X-ray QPO signature in AT 2018cow, if interpreted as an orbital frequency in the accretion disk, furthermore implies $M_\bullet < 850\,M_\odot$. Nevertheless, if the IMBH-TDE is the correct physical scenario powering LFBOTs, we predict that other LFBOTs will be associated with larger disks at late times (e.g., cooler late-time emission). On the other hand, the W–R BH merger scenario that invokes lower-mass BHs offers a natural source of dense CSM within $r \sim$ a few $\times\ 10^{16}$ cm in the form of W–R mass loss and relic disk from the common-envelope phase (Tuna & Metzger 2023), while being able to explain the compact size of the disk at late times of our monitoring. A similar scenario, involving an NS spiraling-in inside the envelope of a massive star, has been proposed by Soker et al. (2019) (see also Grichener 2023).

Most importantly, independently from the BH mass, our work provides support to the hypothesis that LFBOTs are accretion-powered transients, thus also indirectly supporting the picture where the early, luminous, and short-lived UV–optical emission that gives LFBOTs their name originates at least in part from (partial) reprocessing of the high-energy X-rays by outflows launched by the super-Eddington accretion disk. In this accretion-powered scenario the LFBOTs' observational properties at early times represent electromagnetic manifestations of super-Eddington accreting systems, later transitioning into an Eddington-to-sub-Eddington accretion ratio over the timescale of a few hundred days. In this perspective LFBOTs qualify as new laboratories for super-Eddington accretion physics. However, AT 2018cow is still the only event for which meaningful observations and detailed studies of its early- (i.e., $\delta t < 1$ week) *and* late-time (i.e., $\delta t >$ years) evolution can be performed thanks to its proximity. Going forward, wide-field-of-view UV missions like ULTRASAT (Sagiv et al. 2014) and UVEX (Kulkarni et al. 2021) will fill up this observational gap by providing early UV detections of LFBOTs in the local Universe. Finally, if related to an IMBH-TDE, LFBOTs are expected to produce gravitational waves, observable in the future in the local Universe ($\sim$10–25

[28] We note that the highly aspherical geometry invoked here is consistent with the large polarization degree reaching $\sim$7% measured at optical wavelengths at a few days post-discovery of AT 2018cow (Maund et al. 2023).

[29] Specifically we note how IMBHs have been invoked in the ULX literature for systems that later were revealed to host pulsars; see, e.g., King et al. (2023) and references therein.

Mpc) using the LISA detector (e.g., Eracleous et al. 2019, and references therein).

Acknowledgments

The first two authors have equally contributed to the realization of the paper. The authors thank the anonymous referee for constructive suggestions that improved the clarity of the manuscript. This paper is partially based on observations obtained with XMM-Newton, an ESA science mission with instruments and contributions directly funded by ESA Member States and NASA. This material is based on work partially supported by the National Aeronautics and Space Administration under grant/contract/agreement No. 80NSSC22K0898 (PI Margutti). This research has made use of data obtained from the 4XMM XMM-Newton serendipitous source catalog compiled by the 10 institutes of the XMM-Newton Survey Science Centre selected by ESA. G.M. acknowledges financial support from INAF mini-grant "The high-energy view of jets and transient" (Bando Ricerca Fondamentale INAF 2022). R. M. acknowledges partial support by the National Science Foundation under grant Nos. AST-2221789 and AST-2224255 and by the Heising-Simons Foundation under grant No. 2021-3248.

Facilities: HST(STIS), Swift(XRT and UVOT), NuSTAR, XMM, CXO.

Software: astropy (Astropy Collaboration et al. 2013), scipy (Virtanen et al. 2020), XMM-Newton SAS, HEAsoft, XSPEC (Arnaud 1996), CIAO (Fruscione et al. 2006).

Appendix
Early-time Chandra Observations

Chandra observed AT 2018cow with the Low Energy Transmissions Gratings (LETG), using the High Resolution Camera (HRC) spectroscopy detectors for 48 ks, beginning on 2018 June 24 ($\delta t = 8.2$ days). A quick reduction was presented in a telegram shortly after the data were taken (Maccarone & Rivera Sandoval 2018), and our more careful analysis is consistent with that work. We use the TGCAT data reductions (Huenemoerder et al. 2011) and use all orders of the spectrum for ± 1 to ± 8. The initial goal for using this mode was to determine whether there was an extreme-UV excess from this source, given the strong UV emission observed by Swift-UVOT (Kuin et al. 2019; Rivera Sandoval & Maccarone 2018). Such an excess was not present, and the spectrum below about 0.2 keV was heavily dominated by background. We thus fit the data between the chip gap energy and 7 keV. For the negative orders the range of fitted energy is 0.3–7 keV, while for the positive orders it is from 0.24 to 7 keV.

We group the data into bins with at least 100 counts and fit using χ^2 with Gehrels (1986) weighting. Using an absorbed power-law spectrum, with the `Xspec` (Arnaud 1996) `phabs` model within `Sherpa` (Freeman et al. 2001), we find $N_{\rm H} = 5.5^{+3.8}_{-2.7} \times 10^{20}$ cm^{-2} (thus consistent with $N_{\rm H,MW}$), $\Gamma = 1.66^{+0.2}_{-0.17}$, and a total unabsorbed flux from 0.25 to 7.0 keV of $(8.5 \pm 0.7) \times 10^{-12}$ erg s^{-1} cm^{-2}, with χ^2/ν of 136/162. Additional parameters are thus not well justified. The 0.3–10 keV luminosity is $(4.8 \pm 0.4) \times 10^{42}$ erg s^{-1}, and it is in line with the values measured by the other X-ray observatories at the same epoch.

ORCID iDs

Giulia Migliori https://orcid.org/0000-0003-0216-8053
R. Margutti https://orcid.org/0000-0003-4768-7586
B. D. Metzger https://orcid.org/0000-0002-4670-7509
R. Chornock https://orcid.org/0000-0002-7706-5668
C. Vignali https://orcid.org/0000-0002-8853-9611
D. Brethauer https://orcid.org/0000-0001-6415-0903
D. L. Coppejans https://orcid.org/0000-0001-5126-6237
L. Rivera Sandoval https://orcid.org/0000-0002-9396-7215
J. S. Bright https://orcid.org/0000-0002-7735-5796
T. Laskar https://orcid.org/0000-0003-1792-2338
D. Milisavljevic https://orcid.org/0000-0002-0763-3885
E. Berger https://orcid.org/0000-0002-9392-9681
A. J. Nayana https://orcid.org/0000-0002-8070-5400

References

Akashi, M., & Soker, N. 2021, MNRAS, 501, 4053
Antoni, A., & Quataert, E. 2022, MNRAS, 511, 176
Arcavi, I., Wolf, W. M., Howell, D. A., et al. 2016, ApJ, 819, 35
Arnaud, K. A. 1996, in ASP Conf. Ser. 101, Astronomical Data Analysis Software and Systems V, ed. G. H. Jacoby & J. Barnes (San Francisco, CA: ASP), 17
Astropy Collaboration, Robitaille, T. P., Tollerud, E. J., et al. 2013, A&A, 558, A33
Begelman, M. C. 1979, MNRAS, 187, 237
Belloni, T. M., & Motta, S. E. 2016, in Astrophysics and Space Science Library, Vol. 440, Astrophysics of Black Holes: From Fundamental Aspects to Latest Developments, ed. C. Bambi (Berlin: Springer), 61
Bietenholz, M. F., Margutti, R., Coppejans, D., et al. 2020, MNRAS, 491, 4735
Blandford, R. D., & Begelman, M. C. 1999, MNRAS, 303, L1
Brethauer, D., Margutti, R., Milisavljevic, D., et al. 2022, ApJ, 939, 105
Bright, J. S., Margutti, R., Matthews, D., et al. 2022, ApJ, 926, 112
Cannizzo, J. K., Lee, H. M., & Goodman, J. 1990, ApJ, 351, 38
Chen, Y., Drout, M. R., Piro, A. L., et al. 2023a, ApJ, 955, 43
Chen, Y., Drout, M. R., Piro, A. L., et al. 2023b, ApJ, 955, 42
Chevalier, R. A., & Fransson, C. 2017, in Handbook of Supernovae, ed. A. W. Alsabti & P. Murdin (Berlin: Springer), 875
Chrimes, A. A., Jonker, P. G., Levan, A. J., et al. 2024, MNRAS: Letters, 527, L47
Coppejans, D. L., Margutti, R., & Terreran, G. 2020, ApJL, 895, L23
Dessart, L., Hillier, D. J., & Kuncarayakti, H. 2022, A&A, 658, A130
Drout, M. R., Chornock, R., Soderberg, A. M., et al. 2014, ApJ, 794, 23
Eracleous, M., Gezari, S., Sesana, A., et al. 2019, BAAS, 51, 10
Fox, O. D., & Smith, N. 2019, MNRAS, 488, 3772
Frank, J., King, A., & Raine, D. J. 2002, Accretion Power in Astrophysics: Third Edition (Cambridge: Cambridge Univ. Press)
Fransson, C., Lundqvist, P., & Chevalier, R. A. 1996, ApJ, 461, 993
Freeman, P., Doe, S., & Siemiginowska, A. 2001, Proc. SPIE, 4477, 76
Fruscione, A., McDowell, J. C., Allen, G. E., et al. 2006, Proc. SPIE, 6270, 62701V
Fuller, J., & Ma, L. 2019, ApJL, 881, L1
Gehrels, N. 1986, ApJ, 303, 336
Gottlieb, O., Tchekhovskoy, A., & Margutti, R. 2022, MNRAS, 513, 3810
Grichener, A. 2023, MNRAS, 523, 221
Harrison, F. A., Craig, W. W., Christensen, F. E., et al. 2013, ApJ, 770, 103
Ho, A. Y. Q., Margalit, B., Bremer, M., et al. 2022a, ApJ, 932, 116
Ho, A. Y. Q., Perley, D. A., Chen, P., et al. 2022b, TNSAN, 267, 1
Ho, A. Y. Q., Perley, D. A., Kulkarni, S. R., et al. 2020, ApJ, 895, 49
Ho, A. Y. Q., Perley, D. A., Yao, Y., et al. 2022c, ApJ, 938, 85
Ho, A. Y. Q., Phinney, E. S., Ravi, V., et al. 2019, ApJ, 871, 73
Huenemoerder, D. P., Mitschang, A., Dewey, D., et al. 2011, AJ, 141, 129
Inkenhaag, A., Jonker, P. G., Levan, A. J., et al. 2023, MNRAS, 525, 4042
Kalberla, P. M. W., Burton, W. B., Hartmann, D., et al. 2005, A&A, 440, 775
Kara, E., Miller, J. M., Reynolds, C., & Dai, L. 2016, Natur, 535, 388
King, A., Lasota, J.-P., & Middleton, M. 2023, NewAR, 96, 101672
Kitaki, T., Mineshige, S., Ohsuga, K., & Kawashima, T. 2021, arXiv:2101.11028
Kuin, N. P. M., Wu, K., Oates, S., et al. 2019, MNRAS, 487, 2505
Kuin, N. P. M., Wu, K., Oates, S., et al. 2019, MNRAS, 487, 2505

Kulkarni, S. R., Harrison, F. A., Grefenstette, B. W., et al. 2021, arXiv:2111.15608
Lehmer, B. D., Basu-Zych, A. R., Mineo, S., et al. 2016, ApJ, 825, 7
Leung, S.-C., Fuller, J., & Nomoto, K. 2021, ApJ, 915, 80
Lyman, J. D., Galbany, L., Sanchez, S. F., et al. 2020, MNRAS, 495, 992
Maccarone, T. J., Rivera Sandoval, L., Corsi, A. R., Pooley, D., & Knigge, C. 2018, ATel, 11779, 1
Margalit, B. 2022, ApJ, 933, 238
Margutti, R., Kamble, A., Milisavljevic, D., et al. 2017, ApJ, 835, 140
Margutti, R., Metzger, B. D., Chornock, R., et al. 2019, ApJ, 872, 18
Matthews, D. J., Margutti, R., Metzger, B. D., et al. 2023, RNAAS, 7, 126
Maund, J. R., Höflich, P. A., Steele, I. A., et al. 2023, MNRAS, 521, 3323
Metzger, B. D. 2022, ApJ, 932, 84
Metzger, B. D., & Perley, D. A. 2023, ApJ, 944, 74
Metzger, B. D., Piro, A. L., & Quataert, E. 2008, MNRAS, 390, 781
Michałowski, M. J., Kamphuis, P., Hjorth, J., et al. 2019, A&A, 627, A106
Miller, J. M., Fabian, A. C., & Miller, M. C. 2004a, ApJ, 607, 931
Miller, J. M., Fabian, A. C., & Miller, M. C. 2004b, ApJL, 614, L117
Mineo, S., Gilfanov, M., Lehmer, B. D., Morrison, G. E., & Sunyaev, R. 2014, MNRAS, 437, 1698
Mineo, S., Gilfanov, M., & Sunyaev, R. 2012, MNRAS, 426, 1870
Mohan, P., An, T., & Yang, J. 2020, ApJL, 888, L24
Mummery, A., van Velzen, S., Nathan, E., et al. 2024, MNRAS, 527, 2452
Narayan, R., & McClintock, J. E. 2008, NewAR, 51, 733
Narayan, R., & Yi, I. 1995, ApJ, 444, 231
Nayana, A. J., & Chandra, P. 2021, ApJL, 912, L9
Nicholl, M., Srivastav, S., Fulton, M. D., et al. 2023, ApJL, 954, L28
Pasham, D. R., Ho, W. C. G., Alston, W., et al. 2021, NatAs, 6, 249
Pellegrino, C., Howell, D. A., Vinkó, J., et al. 2022, ApJ, 926, 125
Perley, D. A., Mazzali, P. A., Yan, L., et al. 2019, MNRAS, 484, 1031
Poznanski, D., Chornock, R., Nugent, P. E., et al. 2010, Sci, 327, 58
Prentice, S. J., Maguire, K., Smartt, S. J., et al. 2018, ApJL, 865, L3
Pursiainen, M., Childress, M., Smith, M., et al. 2018, MNRAS, 481, 894
Quataert, E., Lecoanet, D., & Coughlin, E. R. 2019, MNRAS, L83, L83
Rest, A., Garnavich, P. M., Khatami, D., et al. 2018, NatAs, 2, 307
Reynolds, C. S. 1999, in ASP Conf. Ser. 161, High Energy Processes in Accreting Black Holes, ed. J. Poutanen & R. Svensson (San Francisco, CA: ASP), 178
Risaliti, G., Harrison, F. A., Madsen, K. K., et al. 2013, Natur, 494, 449
Rivera Sandoval, L. E., & Maccarone, T. 2018, ATel, 11737, 1
Rivera Sandoval, L. E., Maccarone, T. J., Corsi, A., et al. 2018, MNRAS, 480, L146
Rosen, S. R., Webb, N. A., Watson, M. G., et al. 2016, A&A, 590, A1
Sadowski, A., & Narayan, R. 2015, MNRAS, 453, 3213
Sadowski, A., & Narayan, R. 2016, MNRAS, 456, 3929
Sagiv, I., Gal-Yam, A., Ofek, E. O., et al. 2014, AJ, 147, 79
Schrøder, S. L., MacLeod, M., Loeb, A., Vigna-Gomez, A., & Mandel, I. 2020, ApJ, 892, 13
Shakura, N. I., & Sunyaev, R. A. 1973, A&A, 500, 33
Smartt, S. J., Smith, K. W., et al. 2018, ATel, 11727, 1
Soker, N., Grichener, A., & Gilkis, A. 2019, MNRAS, 484, 4972
Stone, N., Sari, R., & Loeb, A. 2013, MNRAS, 435, 1809
Sun, N.-C., Maund, J. R., Crowther, P. A., & Liu, L.-D. 2022, MNRAS, 512, L66
Sun, N.-C., Maund, J. R., Shao, Y., & Janiak, I. A. 2023, MNRAS, 519, 3785
Tampo, Y., Tanaka, M., Maeda, K., et al. 2020, ApJ, 894, 27
Thomas, B. P., Wheeler, J. C., Dwarkadas, V. V., et al. 2022, ApJ, 930, 57
Thomsen, L. L., Lixin Dai, J., Ramirez-Ruiz, E., Kara, E., & Reynolds, C. 2019, ApJL, 884, L21
Traulsen, I., Schwope, A. D., Lamer, G., et al. 2019, A&A, 624, A77
Traulsen, I., Schwope, A. D., Lamer, G., et al. 2020, A&A, 641, A137
Tuna, S., & Metzger, B. D. 2023, ApJ, 955, 125
van Velzen, S., Stone, N. C., Metzger, B. D., et al. 2019, ApJ, 878, 82
Virtanen, P., Gommers, R., Oliphant, T. E., et al. 2020, NatMe, 17, 261
Vurm, I., & Metzger, B. D. 2021, ApJ, 917, 77
Webb, N. A., Coriat, M., Traulsen, I., et al. 2020, A&A, 641, A136
Xiang, D., Wang, X., Lin, W., et al. 2021, ApJ, 910, 42
Yao, Y., Ho, A. Y. Q., Medvedev, P., et al. 2022, ApJ, 934, 104
Yuan, F., & Narayan, R. 2014, ARA&A, 52, 529
Zhang, W., Shu, X., Chen, J.-H., et al. 2022, RAA, 22, 125016